

## Optimization of Engine Valve Parameters Based on Experimental Design and Response Surface Methodology

Yuanyuan Zhang<sup>1,\*</sup>, Sihang Wei<sup>1</sup> and Chenrui Xu<sup>2</sup>

<sup>1</sup>School of Automotive and Rail Transit, Nanjing Institute of Technology, Nanjing 211167, China

<sup>2</sup>School of Electrical Engineering and Computer Science, Technical University of Berlin, Berlin 10623, Germany

Received 30 July 2022; Accepted 19 December 2022

### Abstract

In the range of engine operating speed, a reasonable variable strategy based on variable valve timing and lift can be adopted to improve the engine intake flow, power, and torque. In this study, a 1D engine system model was established, and the accuracy of the simulation model was checked through the bench test results. The intake and exhaust pulsations at the high and low typical speeds were further discussed, and the low speed (4000 rpm) was determined as the boundary for the optimization of relevant parameters. Plackett-Burman (PB) experimental design and variance analysis were used to screen out the important valve timing parameters that affect the output torque of the engine. We further explored these significant variables and their correlation effects through the full factor experiment, and a response surface regression model based on response surface method (RSM) was established. Three-dimensional and contour map analysis was conducted for the four factors with interactive effects to study their interaction effects and optimization direction. The optimized combination level of parameters was evaluated, and the simulation results showed that the torque increased by 5.84%, which was completely matched with the prediction and was accurately located within the confidence and prediction intervals. Therefore, the optimization of engine valve timing parameters based on PB experimental design and RSM can effectively predict and improve engine performance.

*Keywords:* engine system model, valve timing, Plackett-Burman experiment, response surface methodology, parameter optimization

### 1. Introduction

According to the pulsating hydrodynamics of the fuel mixture, the change in the engine valve timing or parameters can improve the working quality of the engine entering the cylinder at different speeds and thus enhance its performance. Variable valve timing (VVT) and variable valve lift (VVL) have been widely used in recent years to improve engine performance through adaptive adjustment of valve timing at partial or full engine speed.

Some leading automobile companies have proposed VVT or VVL commercial technologies by adjusting the cam rotation angle and profile, such as Honda's VTEC (VVT and Lift Electronic Control System), BMW's Double Vanos (Dual Camshaft VVT System), and Toyota's VVT-i (Intelligent VVT). The application of VVT system shows that the continuous variation of valve timing and lift also has adjustment restrictions. Therefore, the concept of fully variable valve train (e.g., electromagnetic and electro-hydraulic valve train) is proposed to improve efficiency, reduce energy consumption, and further enhance engine efficiency. The intake valve system controlled by the electromagnetic mechanism can adjust the valve lift, transition time, valve timing, and even the number of working valves under any given working condition [1-4]. A fully variable valve mechanism with an electro-hydraulic mechanism is used to install a hydraulic actuator between the intake valve and the camshaft. The maximum lift of the intake valve and the continuous change of the intake or exhaust opening with the speed can be achieved by releasing or increasing the oil pressure of the hydraulic actuator [5-7].

In addition to mechanism innovation, the fully variable valve mechanism realizes the control of engine load by adjusting the parameters of the intake or exhaust valves rather than the throttle to adapt to the working speed of the engine [3, 8-9]. The electronically adjustable variable valve mechanism tends to maintain the theoretically optimal intake and exhaust to achieve the effect of natural supercharging. This way significantly improves the intake efficiency, torque, and power of the engine. At the same time, better fuel economy and lower NOx emissions can be achieved by controlling the residual gas in the cylinder during the combustion stroke [10-12].

The motion of the fully variable valve mainly includes three parameters: intake and exhaust phases, valve duration angle, and valve lift. Complex coupling effects are exerted between the parameters. Therefore, establishing an accurate engine system model to obtain the optimal valve timing parameters is difficult. The performance of the non-parametric engine model can generally be predicted through evolutionary algorithms and neural networks [13], and the valve timing parameters and engine speed are taken as the input layer; the output layer comprises engine torque and fuel consumption; the best combination of valve parameters can be obtained in this way [14-16]. The optimal algorithm has been applied to engine performance optimization, but some problems still need to be solved. For example, the accuracy of the model depends largely on the amount of experimental data used during training and adjustment, and the details of the model cannot be completely obtained [17]. Kumar et al. [18] used response surface method (RSM) and artificial neural network (ANN) models to establish an accurate regression model for the mixture of biodiesel and

\*E-mail address: tangyuanyuan1214@163.com

ISSN: 1791-2377 © 2022 School of Science, IHU. All rights reserved.

doi:10.25103/jestr.156.12

alcohol fuels in compression ignition engines. They also combined RSM and ANN to conduct simulation experiments and mix optimization. Uslu [19] compared the optimization of engine performance and emission characteristics of the mixed fuel based on ANN and RSM. The results showed that RSM is superior to ANN in modeling and optimization technology. By contrast, the characteristics of polynomial modeling method based on RSM comprehensively consider the complexity and computational efficiency of the model. For example, RSM uses multiple quadratic regression equations and reasonable design of experiment (DOE) data to establish a model reflecting the relationship between independent and dependent variables. Then, it seeks the best parameters by solving nonlinear multivariable problems. Considerable literature applies RSM to study engine system design or optimization [20-24]. However, few studies involve the control strategy of variable valve system and the optimization of intake and exhaust phases.

This study investigates the optimal valve timing and lift based on RSM and DOE to improve engine performance. The simulation model of the engine system is established and corrected by the test data, and this procedure provides a basis for the subsequent analysis and optimization process. Plackett-Burman (PB) method is used to determine the most significant independent variable affecting torque output, reduce the number of subsequent tests, determine the optimization direction, and improve the efficiency of RSM. The quadratic regression model of response surface is

established. The optimal combination parameters are analyzed and verified through simulation based on the full factor test and RSM prediction optimization results. This way provides a basis for the control mechanism and scheme of the fully variable valve mechanism.

## 2. Simulation Model and Methods

### 2.1 Simulation model of engine system

A 250 cc single cylinder gasoline engine featured with four-stroke and operating variable intake and exhaust valves is the research object, and its 1D simulation system model is developed by the gas dynamics software GT Power based on the mathematical model and measurement results, as shown in Fig. 1. From the intake boundary of the model, the airflow passes through the air filter, throttle, intake manifold pipe, intake valve, intake port, and eventually enters the cylinder. After the combustion stroke, the exhaust gases pass through the exhaust port, exhaust manifold pipe, exhaust muffler, and finally exits the exhaust boundary of the system.

The specific geometric parameters of the engine are obtained from experimental measurements and the specifications, which are shown in Table 1. Other input parameters, such as intake and exhaust flow coefficient, throttle flow coefficient, pipe's frictional coefficient, engine's frictional mean effective pressure, combustion heat release rate, and air-fuel ratio, are determined through tests based on steady flow and powertrain dynamic test bench.

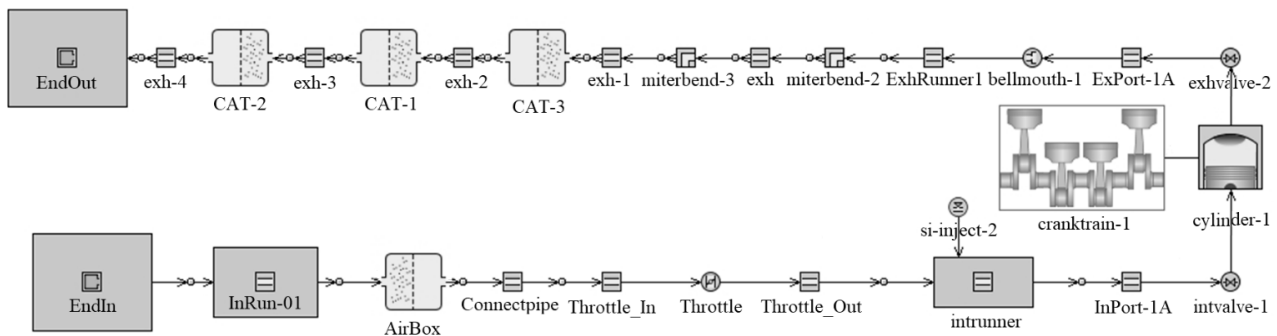


Fig. 1. GT-power model map of the engine

Table 1. Specification of the engine

Number of cylinder	1
Number of valves	2
Displacement	125 cm <sup>3</sup>
Bore	56.5 mm
Stroke	49.5 mm
Maximum power	7.5 kw/9000 rpm
Maximum torque	8.6 N·m/7000 rpm
Valve timing	Intake valve opening 0 °CA BTDC Intake valve closing 30 °CA ABDC Exhaust valve opening 30 °CA BBDC Exhaust valve closing 0 °CA ATDC
Compression ratio	9.2:1
Fuel type	Indolene
Aspiration	Naturally aspirated
Cooling system	Air-cooled

As for the advanced submodules, the injection model is InjAFSeqConn with air-fuel ratio and injection pulse width acquired from experiments, and the heat transfer coefficient is calculated using the heat transfer model proposed by Woschni in 1987 (WoschniGT). The friction and pressure loss of the pipeline are adopted from the Chen-Flynn model, with the friction loss pressure as a function of the piston speed and the peak pressure. Notably, the template of intake

and exhaust cams should be defined as solenoid-actuated valve with adjustable parameters to meet the requirements of VVT, valve lift, and valve overlap during the optimization process correspondingly. However, these variable operating working conditions may cause unexpected influence on combustion. Compared with the non-predicted SI-Wiebe combustion model, SI-Turb model comprehensively considers the cylinder temperature and pressure, in-cylinder mixture composition, valve timings, spark advance angle, fuel properties, and other factors for prediction. In addition, the combustion process can be automatically adjusted as the transient environment changes instead of a large amount of experimental data input, which explains the reason for choosing SI-Turb model. Consequently, more accurate quasi-3D predictable combustion model SI-Turb is established in the 1D model.

The established simulation model needs to be calibrated through the test result data to ensure the reliability of the simulation model. The engine is loaded with the dynamometer, which is mounted on the test bench, and the throttle is set as fully open. Experiments are conducted with the engine rotation speed varying from 2000 rpm to 8500 rpm at 100 rpm intervals. Thereafter, simulation and

experimental values are compared for adjustment and validation. The power, torque, and brake specific fuel consumption (BSFC) curve versus engine rotation speed, are shown in Fig. 2. It shows the consistency between the simulation and experimental results, with the maximum error of BSFC less than 4% and that of torque and power less than 3%. Therefore, the established simulation model is validated to be employed as the basic model for further study.

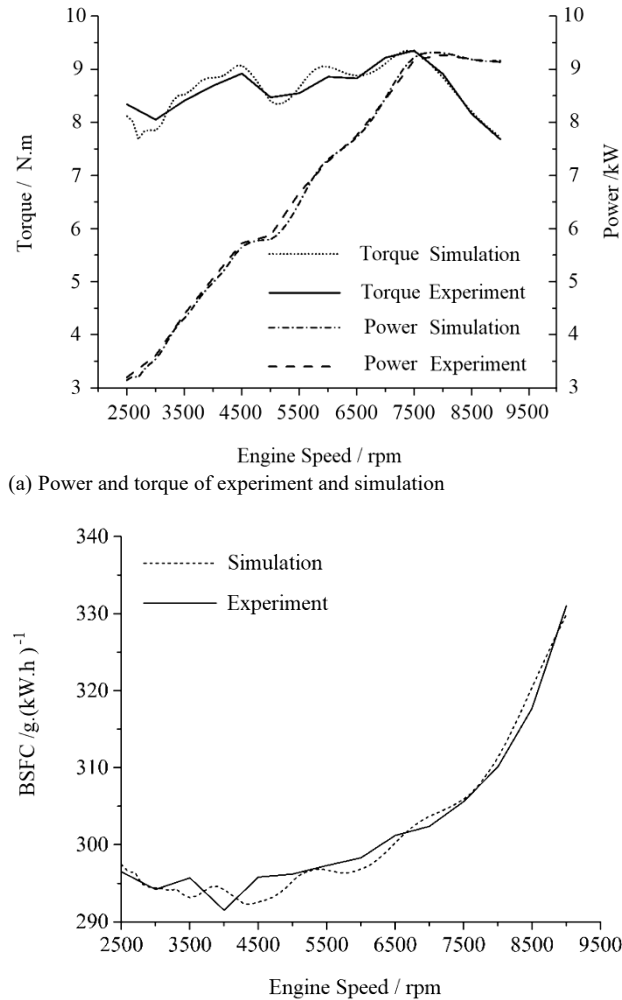


Fig. 2. Comparison between experiment and simulation under full load

Fig. 3 shows the comparison of the intake and exhaust mass flow rate in cylinder at 4000 rpm and 7000 rpm. Notably, the phenomenon of intake backflow during the compression stroke is comparatively more obvious at 4000 rpm, although the valve overlay angle results in slight backflow at both engine speeds. The pressure wave and pulsating flow of intake and exhaust are not in concert with the valve timing. This condition is detrimental to the performance of the engine given that more volume of intake backflow means increasing residual gas and less fresh charge of air fuel for combustion. As a result, this study mainly focuses on the analysis of influence of valve parameters on the torque at the engine speed of 4000 rpm with full load of this engine and the optimization of performance correspondingly.

### 2.2 Design and analysis of the experiment

PB experiment design selects representative experimental points by taking high and low levels for each variable to screen multiple related target variables. The number of

factors is required to be less than the number of experiments to evaluate the error. It is suitable for the case of mixed two-factor interaction of main effects and is fast and efficient.

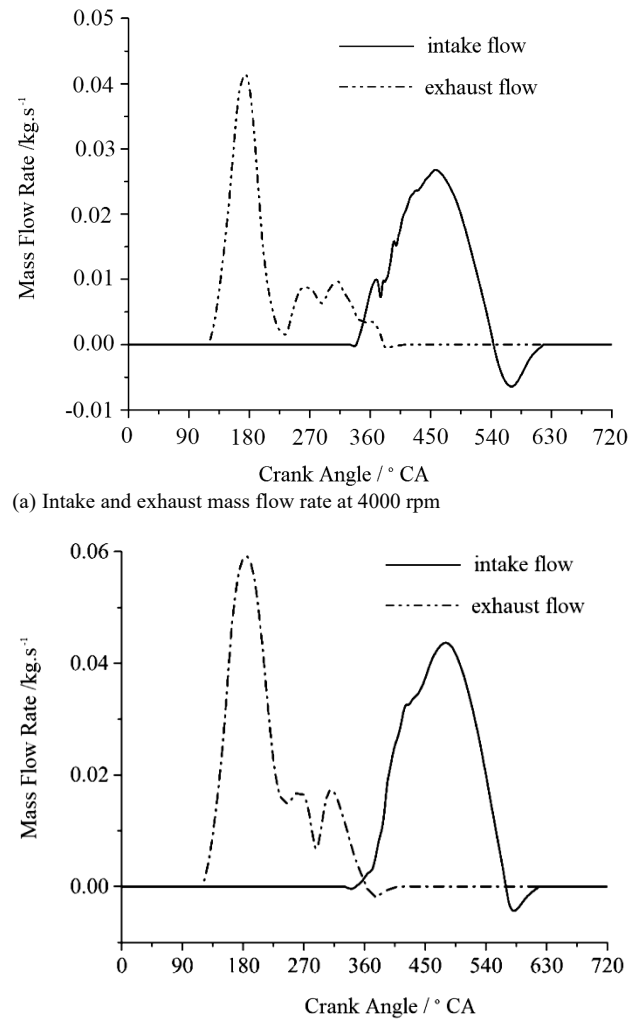


Fig. 3. Comparison of intake and exhaust mass flow in a cylinder at 4000 rpm and 7000 rpm

Based on the abovementioned 1D engine system model, the valve distribution parameter variables are defined as follows: intake advance angle ( $X_1$ ), intake duration angle ( $X_2$ ), intake valve lift ( $X_3$ ), exhaust advance angle ( $X_4$ ), exhaust duration angle ( $X_5$ ), and exhaust valve lift ( $X_6$ ). The movement behavior of intake and exhaust valves is also described in detail. PB design is applied to comprehensively consider the influence of variables and their coupling relationship, reduce the number of tests, improve the efficiency and quality of optimization, and make the optimization close to the optimal or expected value. The impact level of each variable includes high and low, which are coded by +1 and -1, respectively, as shown in Table 2.

Table 2. Level definition of all factorial test design data

Code	Independent Variables /Control Factors	Low Level (-1)	High Level (1)
$X_1$	Intake advance angle	315	375
$X_2$	Intake duration angle	210	285
$X_3$	Intake valve lift	4	8
$X_4$	Exhaust advance angle	140	195
$X_5$	Exhaust duration angle	250	300
$X_6$	Exhaust valve lift	4	8

According to the established model, the output parameters under different gas distribution parameter combinations, such as torque and BSFC, are obtained. Table 3 shows the corresponding numerical factors and output responses, as well as the 12-run PB experimental design matrix generated by the design expert software.

**Table 3.** Design matrix of PB experiment and corresponding BSFC and torque of each run

NO. of Run	X <sub>1</sub>	X <sub>2</sub>	X <sub>3</sub>	X <sub>4</sub>	X <sub>5</sub>	X <sub>6</sub>	Torque	BSFC
1	-1	1	1	1	-1	-1	4.48	327.68
2	-1	1	1	-1	1	1	8.62	301.21
3	1	-1	1	1	-1	1	6.31	309.94
4	1	-1	1	1	1	-1	6.12	315.44
5	-1	-1	1	-1	1	1	9.79	299.13
6	1	-1	-1	-1	1	-1	6.45	312.47
7	1	1	-1	1	1	1	1.08	514.16
8	-1	1	-1	1	1	-1	3.48	344.22
9	1	1	1	-1	-1	-1	4.07	343.26
10	1	1	-1	-1	-1	1	3.83	355.50
11	-1	-1	-1	1	-1	1	4.54	324.94
12	-1	-1	-1	-1	-1	-1	8.74	296.92

The analysis of variance (ANOVA) with reference to *F*-test is used to screen the factors of great significance and explore contribution of each factor to response value variably from the results of PB design. The mathematical model of ANOVA is established based on three fundamental assumptions.

$$1) x_{ij} = \mu + a_i + \varepsilon_{ij} = \mu_i + \varepsilon_{ij} (i = 1, 2, \dots, p; j = 1, 2, \dots, n);$$

$$2) \sum_{i=1}^p a_i = 0;$$

3) Error terms of each factor's level remain independent to each other while following a normal distribution.

where  $x_{ij}$  is the response value under  $j$ th repeated experiment and  $i$ th level of the control factor;  $p$  is the number of the levels of each factor;  $\varepsilon_{ij}$  is the error terms;  $\mu_i$  is the truth value of control factor with  $i$ th level;  $\mu$  is the grand mean of  $\mu_i$ ;  $a_i$  is the deviance of  $\mu_i$  in terms of  $\mu$ .

The residual plot needs to be checked before the ANOVA. Fig. 4 shows the residual plots of torque gained from PB experimental design. The results show that normal probability is nearly a straight line, while the histogram of residuals is similar to the normal distribution plot. Moreover, the structureless plot of residuals versus fits implies that residuals of all dependent variables should have constant variance and that of residuals versus order indicates the assumption that the residuals are independent to each other.

The output response variables are diverse and are affected by the main effects of control factors and the random noise (random error term), which are described as  $S_A$  and  $S_e$ .

$S_A$  (sum of squares between groups) is calculated as

$$S_A = \sum_{i=1}^p \sum_{j=1}^r (\bar{x}_i - \bar{x})^2 = r \sum_{i=1}^p (\bar{x}_i - \bar{x})^2 \quad (1)$$

$S_e$  (sum of squares within groups) is calculated as

$$S_e = \sum_{i=1}^p \sum_{j=1}^r (x_{ij} - \bar{x}_i)^2 \quad (2)$$

*F* value is defined as

$$F = \frac{S_A / f_A}{S_e / f_e} = \frac{S_A / (p-1)}{S_e / (N-p)} = \frac{\bar{S}_A}{\bar{S}_e} \quad (3)$$

where  $f_A$  is the degree of freedom of  $S_A$ ;  $f_e$  is the degree of freedom of  $S_e$ ;  $N$  is the number of same output response by all factors with whole levels;  $\bar{S}_A$  is mean square between groups;  $\bar{S}_e$  is mean square within groups.

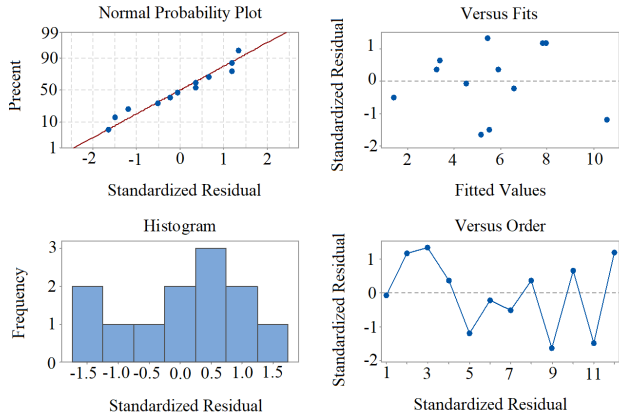


**Fig. 4.** Residual plot obtained from PB experimental design data

After the *F* value is calculated, comparison with  $F_\alpha (f_A, f_e)$ , which is the critical value of *F*, is indispensable to determine the contribution of this factor to the response variable ( $\alpha$  value, which represents the level of significance, is assigned based on the testing precision, as a result of which various values of  $F_\alpha (f_A, f_e)$  can be queried on the table of *F* distribution). If *F* is greater than  $F_\alpha (f_A, f_e)$ , then this control factor is considered affecting the response dramatically. In this study,  $\alpha$  value is defined as 0.05. Table 4(a)-(b) show ANOVA and significance test for response variables of torque ( $Y_1$ ) and BSFC ( $Y_2$ ) at the engine speed of 4000 rpm, respectively. Factors of statistically considerable effect on response variable are selected on condition that *p* value from the results of significance test is less than 0.05. However, the *p* value is greater than 0.05, which implies that the probability of relative factor influencing the response is negligible.

**Table 4. (a)** ANOVA of torque obtained from PB design

Source	Df	Sum of squares	Mean square	<i>F</i> value	<i>P</i> value
Model	6	65.6127	10.9355	10.62	0.010
X <sub>1</sub>	1	11.5506	11.5506	11.22	0.020
X <sub>2</sub>	1	22.3908	22.3908	21.74	0.006
X <sub>3</sub>	1	10.5630	10.5630	10.26	0.024
X <sub>4</sub>	1	19.9887	19.9887	19.41	0.007
X <sub>5</sub>	1	1.0632	1.0632	1.08	0.356
X <sub>6</sub>	1	0.0564	0.0564	0.05	0.824
Residual	5	5.1494	1.0299	—	—
Total	11	70.7622	—	—	—

**Table 4. (b)** ANOVA of BSFC obtained from PB design

Source	Df	Sum of squares	Mean square	<i>F</i> value	<i>p</i> value
Model	6	27652	4609	2.19	0.204
X <sub>1</sub>	1	5491	5491	2.61	0.167
X <sub>2</sub>	1	8921	8921	4.24	0.095
X <sub>3</sub>	1	5273	5273	2.51	0.174
X <sub>4</sub>	1	4327	4327	2.06	0.211
X <sub>5</sub>	1	1374	1374	0.65	0.456
X <sub>6</sub>	1	2266	2266	1.08	0.347
Residual	5	10521	2104	—	—
Total	11	38173	—	—	—

With estimators obtained from PB design, polynomial equations in terms of all factors based on first-order linear model are given as

$$Y_1 = 27.49 - 0.03270X_1 - 0.03643X_2 + 0.469X_3 - 0.0469X_4 + 0.0119X_5 + 0.034X_6 \quad (4)$$

$$Y_2 = 0.713X_1 + 0.727X_2 - 10.48X_3 + 0.691X_4 + 0.428X_5 + 6.87X_6 - 301 \quad (5)$$

Fig.5 shows the standardized Pareto chart of main effects for different response variables. Standardized Pareto charts of all response variables serve as confirmation of the results from ANOVA of PB design. The Pareto charts sequence the standardized effects by significance. The reference line (position depends on  $\alpha$  value) is the statistical significance influence of standard screening.

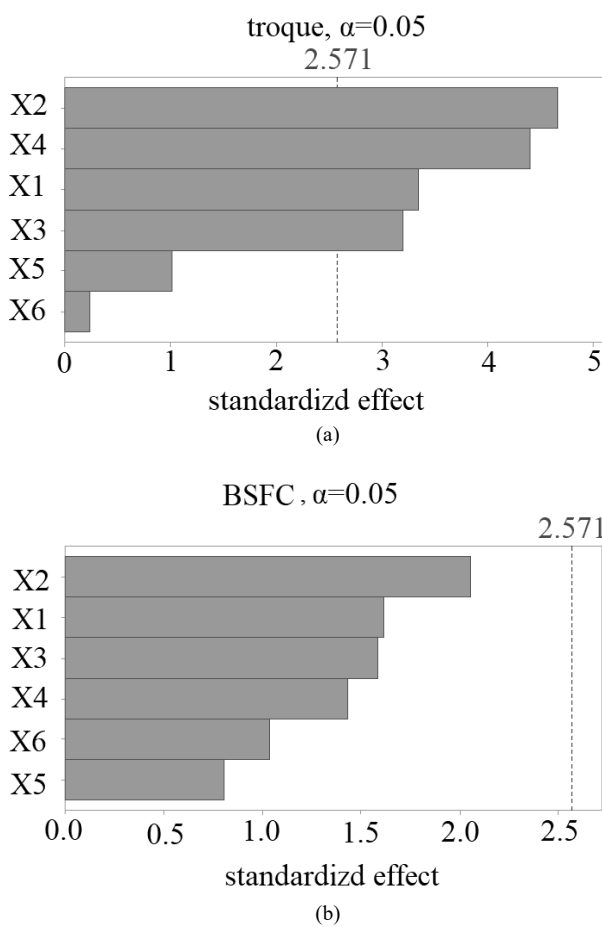


Fig. 5. Standardized Pareto chart of main effects for PB experiment

The results show that intake advance angle, intake duration angle, intake valve lift, and exhaust advance angle are the main affecting factors of torque response. By contrast, the exhaust valve lift and exhaust duration angle have no significant effect. In the next RSM optimization process, the main factors with significant influence will be further studied. The ANOVA results also reveal no significant affecting factors of BSFC ( $p < 0.05$ ), which implies that RSM model is incapable to BSFC.

### 2.3 Establishment of RSM model

The RSM is used to conduct optimization experiments, study the correlation between variables, establish a second-order continuous function model reflecting the relationship

between indicators and variables, and replace the original model solved by intensive computing. Notably, the optimal experimental points need to be included in the experimental design variables when using the RSM. Therefore, different value ranges of variables may lead to unsatisfactory optimization results of the RSM. The steepest rise method can be used to determine the reasonable range of experimental variables. If the current range of valve timing variables is close to the optimal region, then a second-order model is used to find the optimal combination of experimental input variables. For the engine system design problem, the approximate accuracy of the response surface of the second-order polynomial model is generally sufficient, as shown in (6):

$$Y = \beta_0 + \sum_{i=1}^m \beta_i x_i + \sum_{i=1}^m \beta_{ii} x_i^2 + \sum_{i < j} \beta_{ij} x_i x_j + \varepsilon \quad (6)$$

where  $\beta_0$  represents constant term;  $\beta_i$  is the constant coefficient of linear effect of independent variable  $x_i$ ;  $\beta_{ii}$  is the constant coefficient of quadratic effect of the independent variable  $x_i^2$ ;  $\beta_{ij}$  represents the constant coefficient of interaction effect between independent variable  $x_i$  and  $x_j$ ;  $\varepsilon$  is the observation error or random noise supposed to be dependent to each other with mean value;  $\sigma^2$  variance under various experiments.  $Y$  is the dependent variable, which is also referred to as output response value, under the application and control of these diversely combined independent variables.

Constant coefficients of  $\beta_0, \beta_i, \beta_{ii}, \beta_{ij}$  are evaluated by moving least square method (MLS). The approximating function of MLS employs the polynomial of  $n$  degree ( $n < m$ ) as base vector to approach and fit the real one.

$$\begin{cases} f(x) = \sum_{i=1}^m p_i(x) \beta_i(x) = p^T(x) \beta(x) \\ p^T(x) = [p_1(x), p_2(x), \dots, p_m(x)] \end{cases} \quad (7)$$

where  $\beta_i(x), i = 0, 1, \dots, n$  is the vector of undetermined constant coefficients;  $p^T(x)$  denotes a set of base vectors in polynomial space with  $m$  dimensions. Specifically,  $p(x)$  in this study includes constant, linear, powers, and cross products of those base vectors, that is,  $p(x) = [1, x, y, x^2, y^2, xy]$ .

The assumption is that the compact set  $\Omega_x$  of the single calculation point  $x$  from approximating function contains  $N$  nodes. Thereafter, weighted sum of squares of errors can be obtained by

$$J = \sum_{j=1}^n w(x_j) [f(x) - y_j]^2 = \sum_{j=1}^n w(x_j) [p^T(x) \beta(x) - y_j]^2 \quad (8)$$

where  $f(x)$  is the approximating function;  $w(x_j)$  is the weight function with compact support;  $y_j$  is the measured value when  $x = x_j$ , that is,  $y_j = y(x_j)$ ;  $n$  is the actual number of nodes in the whole compact set.

To estimate the undetermined coefficients  $\beta_x$  while using MLS method, the derivation of  $J$  with respect to  $\beta_x$  is calculated in the case that  $J$  is minimized:

$$\frac{\partial J}{\partial \beta} = A(x)\beta(x) - B(x)y = 0 \Rightarrow \beta(x) = A^{-1}(x)B(x)y \quad (9)$$

The results are given as

$$\begin{cases} y = [y_1, y_2, \dots, y_n]^T \\ A = \sum_{j=1}^n w(x_j) p(x) p^T(x) \\ B = [w(x_1) p(x_1), w(x_2) p(x_2), \dots, w(x_n) p(x_n)] \end{cases} \quad (10)$$

Following prerequisites must be satisfied to select weight function  $w_i(x)$ .

- (1)The weight function value should be nonnegative, that is,  $w(x-x_i) > 0$  in the compact set while  $w(x-x_i) = 0$  beyond the compact set;
- (2)The weight function should be monotonically decreasing with increasing distance away from  $x$ ;
- (3)The weight function should be sufficiently smooth, particularly at the boundary of compact set.

Consequently, normal weight function is adopted in this study.

$$w(r, \sigma) = \begin{cases} \frac{1}{\sqrt{2\pi}\sigma} \exp\left(-\frac{1}{2}\left(\frac{r}{\sigma}\right)^2\right), r \leq 1 \\ 0, r > 1 \end{cases} \quad (11)$$

Compared with PB experimental design, full factorial experimental design can comprehensively evaluate the impact of interaction between different variables. Thus, it can establish a higher-order response surface model. The mixed level full factor design test with four variables (i.e., intake valve opening, intake opening duration, intake valve lift, and exhaust early opening angle) is adopted. The level of each variable is shown in Table 5.

**Table 5.** Full factorial experiment design

Coded Level	Independent Variables/Control Factors			
	$X_1/^\circ$	$X_2/\text{mm}$	$X_3/^\circ$	$X_4/^\circ$
1	315	215	4	135
2	330	224	5	150
3	345	233	6	165
4	360	242	7	180
5	375	250	8	195

Significance test needs to be conducted for the quadratic regression model to ensure the reliability and adaptability of the established response surface model and enhance its effectiveness of prediction. In this work,  $F$  test, similar to the ANOVA conducted above, of the regression model is conducted based on the null hypothesis that followed and the  $\alpha$  value is also defined as 0.05.

$$\begin{aligned} H_0 : \mu_0 = \mu_1 = \mu_2 = \dots = \mu_k \\ H_1 : \mu_j (j = 1, 2, 3 \dots k) \neq 0 \text{ (for at least one } j) \end{aligned}$$

$$S_{ST} = S_{SR} + S_{SE} \quad (12)$$

where  $S_{ST}$  is the sum of squares in total,  $S_{SR}$  is the regression or the sum of squares to be explained, and  $S_{SE}$  is the sum of squares due to errors or residual sum of square.

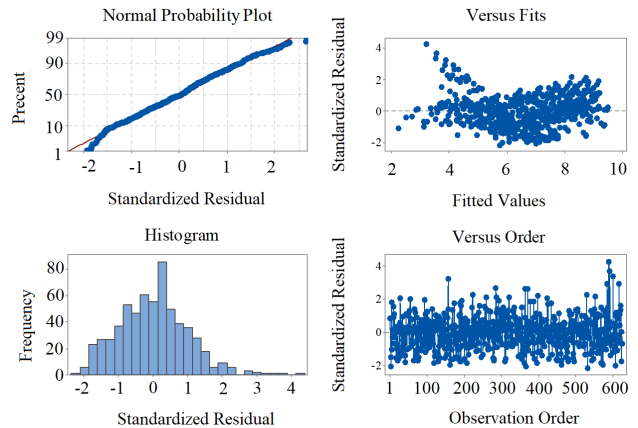


**Fig.6.** Residual plot obtained from the full factorial experimental design data

$$F = \frac{MS_R}{MS_e} = \frac{SS_R / m}{SS_e / n - m - 1} \quad (13)$$

where  $m$  is the number of the independent variables of the regression model and  $n$  is the number observations of the experiment. The calculated  $F$  value is compared with critical value of  $F$ , that is,  $F_\alpha(m, n-m-1)$ ; if the  $F$  value is greater or  $p < \alpha$ , then the null hypothesis is rejected, which results in that at least one independent variable can explain and affect the model significantly.

The observation errors of response surface are supposed to be dependent on each other with mean value and  $\sigma^2$  variance. Thus, the residual plot needs to be checked before the significance test. Fig. 6 shows the residual plots of torque gained from full factorial experimental design. The analysis error of the residual diagram is normally distributed and independent of each other, while the variance remains unchanged under various experiments.

Normally, the coefficient of multiple determination ( $R^2$ ), the adjusted coefficient of determination ( $R^2_{adj}$ ), and the predicted coefficient of determination  $R^2_{pred}$  are adopted to serve as evaluation indicators of the established regression model. If the number of independent variables or other items is added, then the correlation coefficient  $R^2$  can be used for evaluation. However, the model fitting effect may not be improved. To obtain better fit and prevent over fitting,  $R^2_{adj}$  makes reasonable compensation for the added variables and comprehensively considers the effect of sample size and independent variables on the model fitting.  $R^2_{pred}$  represents the prediction ability of the original regression model that is synthesized by running all permutations of  $n$  observations.  $R^2_{pred}$  is a more practical and useful evaluation index than  $R^2$  and  $R^2_{adj}$ , and it can be used to judge the quality of the regression model. In any case,  $R^2_{adj}$  should not be greater than  $R^2$ .

Multiple determination:

$$R^2 = \frac{S_{SR}}{S_{ST}} = \frac{S_{SR} - S_{ST}}{S_{ST}} = 1 - \frac{\sum_{i=1}^n (\hat{y} - y_i)^2}{\sum_{i=1}^n (y_i - \bar{y})^2} \quad (14)$$

Adjusted coefficient of determination:

$$R^2_{adj} = 1 - \frac{S_{SE} / (n - m - 1)}{S_{ST} / (n - 1)} = 1 - \frac{n - 1}{n - m - 1} (1 - R^2) \quad (15)$$

Predicted coefficient of determination:

$$R^2_{pred} = 1 - \frac{U_{PRESS}}{S_{ST}} = 1 - \frac{\sum_{i=1}^n (y_i - \hat{y}_i)^2}{\sum_{i=1}^n (y_i - \bar{y})^2} \quad (16)$$

where  $U_{PRESS}$  is the predicted residual error sum of squares,  $n$  is the number of observation samples in the experiment,  $p$  is the number of different items in the response model,  $y_i$  is the value of  $i$ th observation to be predicted by the response model,  $\bar{y}$  is mean value of all the observations, and  $\hat{y}$  is the predicted value of  $i$ th observation.

In general, the value of  $R^2_{pred}$  for a model with acceptable accuracy should be greater than 0.8 to 0.9, and the difference between  $R^2_{pred}$  and  $R^2$  should not be greater than 0.2 to 0.3.

However, the significance of each independent variable and interactive term remains unknown given that distinguishing which term has significant effect on dependent variables only by the F test of regression model is difficult. Therefore, after the quadratic regression is tested as significant, coefficients of regression model must go through the significance test one by one to determine and remove the insignificant coefficients and corresponding terms. This way simplifies the model to reduce the residual and standard deviation of the model and improve the fitting accuracy.

After insignificant terms are deleted grounded on the F test and estimators are obtained from full factorial experimental design, polynomial equations of four dependent variables based on second-order regression model are given as

$$Y_1 = 0.9032X_1 + 0.5163X_2 + 0.577X_3 - 0.07228X_4 - 0.001143X_1^2 - 0.000431X_2^2 - 0.03345X_3^2 - 0.000730X_4^2 - 0.001103X_1X_2 - 0.000557X_1X_3 + 0.000756X_1X_4 + 0.001058X_3X_4 - 189.64 \quad (17)$$

Table 6 shows that the interactive terms of the four independent variables  $X_1X_2$ ,  $X_1X_3$ ,  $X_1X_4$ , and  $X_3X_4$  with p value smaller than 0.05 play an important role for the output response variable of torque. The values of  $R^2_{adj}$ ,  $R^2_{pred}$ , and  $R^2$  are all higher than 0.98, and the difference between the values of  $R^2_{pred}$  and  $R^2$  is far less than the critical range value of 0.2-0.3. Therefore, the model has strong predictive ability.

**Table.6.** Regression analysis of quadratic model based on full factorial experiments

Source	Df	Sum of squares	Mean square	F value	p value
Model	12	1448.87	120.7	3909.00	<0.000
$X_1$	1	121.24	121.24	3925.11	<0.000
$X_2$	1	404.33	404.33	13090.43	<0.000
$X_3$	1	31.29	31.29	1012.91	<0.000
$X_4$	1	595.09	595.09.03	19266.33	<0.000
$\sum_{i=1}^4 X_i^2$	4	166.80	41.70	1350	<0.000
$X_1 X_2$	1	53.02	53.02	1716.49	<0.000
$X_1 X_3$	1	0.17	0.17	5.64	0.018
$X_1 X_4$	1	72.27	72.27	2339.74	<0.000
$X_3 X_4$	1	0.63	0.63	20.38	<0.000
Residual	13	18.90	0.031	—	—
Total	624	1467.77	—	—	—

$$R^2_{adj}=0.9869, R^2_{pred}=0.9865, R^2=0.9871$$

### 3. Results Analysis

Other parameters are kept at an intermediate level, the influence of combination of double valve train parameters on torque is determined, and 3D surface and contour maps are taken as the object for analysis. Contour plots are used to directly represent the effect of variables on the output torque. The 3D surface graph reflects the shape of the regression function of the response surface model. Specifically, the interaction between variables is positively related to the curvature of the surface. The degree of interaction can be inferred from the shape of the contour. The elliptical contour graph indicates a strong interaction between variables, while the circle implies the opposite.

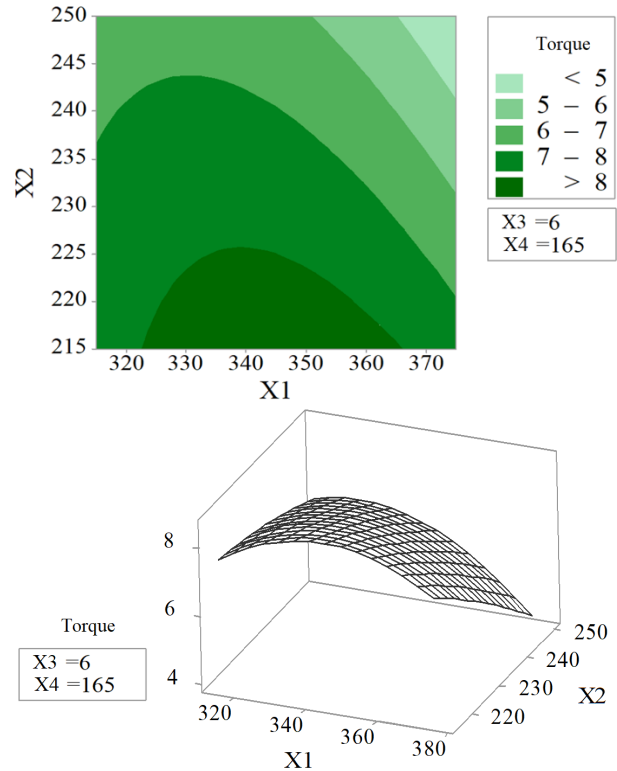


**Fig. 7.** 3D surface and contour plots of the effect of intake advance and duration angles

Fig.7 shows the surface and contour plots of the influence of intake advance and duration angles. The results show that the intake duration angle is highly sensitive to torque. The closing angle of intake valve can be calculated through the opening duration of intake valve and its early opening angle. The closing angle of intake valve lagging behind the bottom dead center can increase the intake air volume by using the intake air flow inertia and the negative pressure in the cylinder. If the lag angle is too large, then gas backflow will occur. For the optimization of torque at 4000 rpm, the late closing angle of intake valve has an optimal value, which is achieved at 340°. Therefore, the original intake advance angle is unsuitable for this engine speed and should be reduced appropriately to obtain better torque performance.

Fig. 8 shows that intake advance angle and intake valve lift have a significant interaction effect on torque. The short axis of the ellipse is located in the coordinate axis direction of the intake advance angle, which indicates that the intake advance angle has more effect on the torque change than the intake valve lift. In the whole range, the torque increases with the rise in the intake valve lift. This increasing trend

expands the flow area of the intake air. Thus, the resistance and pumping loss are reduced when sucking in air and fuel at this engine speed. The torque reaches the peak when the intake advance angle is about 335°. The contour map is sparse and the curvature of the surface map is large when the intake advance angle is greater than 350° and far from the optimal area. This finding shows that the torque does not change significantly near its optimum region.

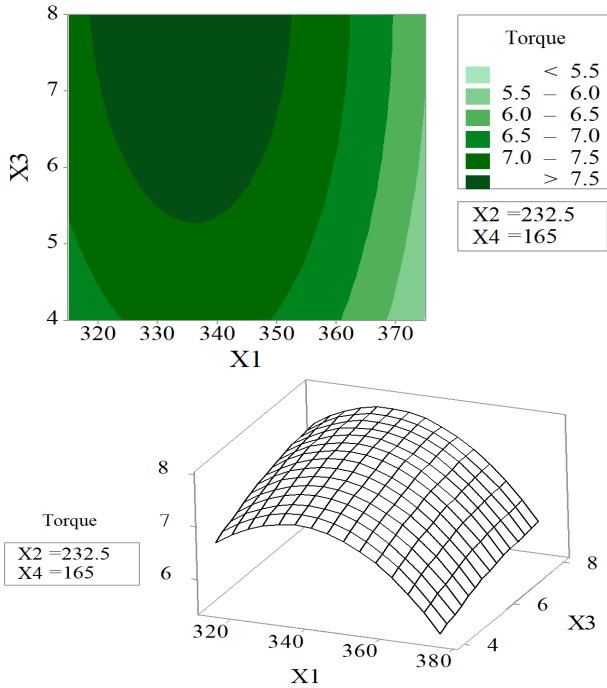


Fig. 8. 3D surface and contour plots of the effect of intake advance angle and intake valve lift

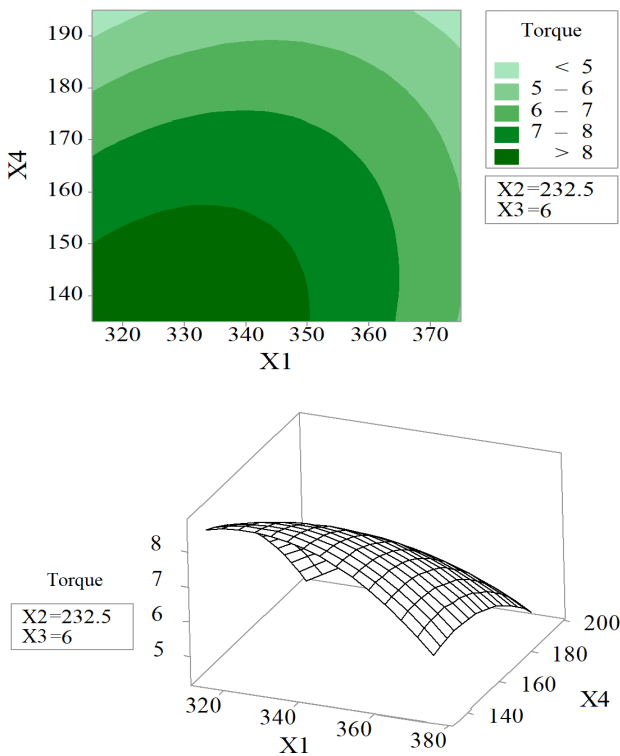


Fig. 9. 3D surface and contour plots of the effect of intake and exhaust advance angles

Fig. 9 shows that the torque increases with the decrease in intake and exhaust advance angles. Torque is more sensitive to exhaust advance angle than intake advance angle. A larger exhaust advance angle will help exhaust the combustion gas rapidly by using the expansion in the cylinder and the combustion pressure, which significantly reduces the residual exhaust mass. With the increase in intake advance angle, the sensitivity of torque to exhaust advance angle decreases significantly, especially when the intake advance angle exceeds 350°. When the exhaust advance angle exceeds 150°, the torque no longer changes monotonously, and a peak value is observed in the whole range. The interaction between the two variables is relatively weak.

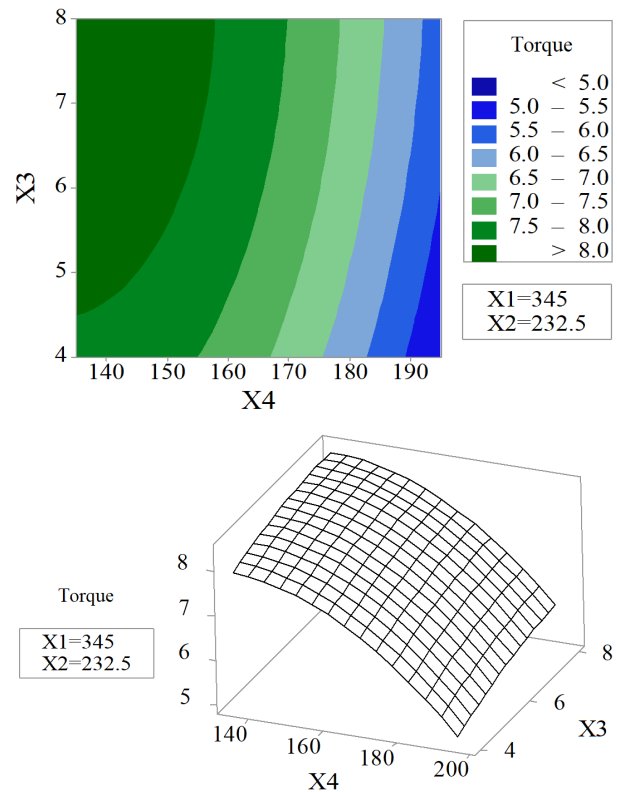


Fig. 10. 3D surface and contour plots of the effect of intake valve lift and exhaust advance angle

Fig. 10 shows that torque is more sensitive to the exhaust advance angle than the intake valve lift, and the interaction effect between them is significant given that the contour map is oval. When the exhaust advance angle is greater than 155°, the sensitivity of the relative torque increases rapidly, which means that the torque changes very little during the optimal combination of the exhaust advance angle and the intake valve lift. As the exhaust advance angle decreases and the intake valve lift increases, the torque will also rise.

The output torque is further optimized based on the quadratic regression model and the analysis of four independent variables involving valve timing to achieve better power performance while other settings are kept constant. This optimization process is conducted by employing response optimizer provided by statistical software Minitab. Each response variable is transformed into a dimensionless desirability to evaluate the results of the response optimization under diverse settings of weight and importance. The individual desirability ranges from zero to one: zero means the optimized response is completely beyond acceptable constraints, while one means the

optimized response result is ideal. Optimization directions of the response variable are divided as not to optimize, maximize, target, and minimize.

The individual desirability of maximizing target value is obtained by the function given as

$$d_i = \begin{cases} 0, & y_i > l_i \\ [(y_i - l_i) / (t_i - l_i)]^{w_i}, & l_i \leq y_i \leq t_i \\ 1, & y_i > l_i \end{cases} \quad (18)$$

where  $y_i$  is the response value predicted of  $i$ th observation,  $l_i$  is the lowest acceptable response value of  $i$ th observation,  $w_i$  is the weight assigned for this response variable, and  $t_i$  is target value of  $i$ th observation.

This optimization procedure aims to improve the performance of the engine. Specifically, torque is maximized with optimization criterion constraints of four independent variables of valve timing. The weight and importance of the desirability function are both set to 1. The maximum torque and optimized combination of independent variables of valve timing under this circumstance are predicted by optimization of the established RSM model, as shown in Table 7.

**Table 7.** Validation of optimization by RSM at 4000 rpm

Optimized				Predicted	Test	Error	$d$
$X_1$	$X_2$	$X_3$	$X_4$				
333.8	215	8	135	9.523	9.517	0.06%	0.997

The results show that the maximum output torque is 9.523 N·m with 95% confidence interval of 9.46-9.58, 95% prediction interval of 9.17-9.87, and standard error of the fits of 0.03 for the optimized level of valve timing parameters. The results are further verified by simulation, and the optimization results are compared with the original engine settings. The torque directly calculated by simulation confirms the optimization effect. The torque directly calculated from simulation confirms the optimization effect by increasing torque to 9.517 N·m with an error of 0.06%, which perfectly matches the prediction and is positioned exactly within the confidence and prediction interval. Consequently, the quadratic regression model in terms of torque established based on RSM accurately reflects the correlation between the torque and parameters of valve timing and is of high reliability and prediction accuracy. The individual desirability of maximizing target value is 0.997, which implies strong optimization effects.

Fig. 11 shows the comparison of torque, power, and mass flow rate of intake flow obtained from simulation before and after optimization at 4000 rpm. The torque and power are improved with optimized valve timing by RSM during low engine speed, particularly under 4800 rpm. Specifically, torque increases from 8.99 N·m to 9.51 N·m with a growth rate of 5.84% by optimization at 4000 rpm, although BSFC is also increased only 0.32% from 294.18  $g \cdot (Kw \cdot h)^{-1}$ . This result is mainly due to reduction in intake backflow during compression stroke caused by the increased intake valve closing angle according to the optimized valve timing configuration, although overlap angle also leads to more backflow at the same time as is indicated by the comparison plot of intake mass flow rate. The origin configuration of valve timing is more suitable for high-speed interval of the engine.

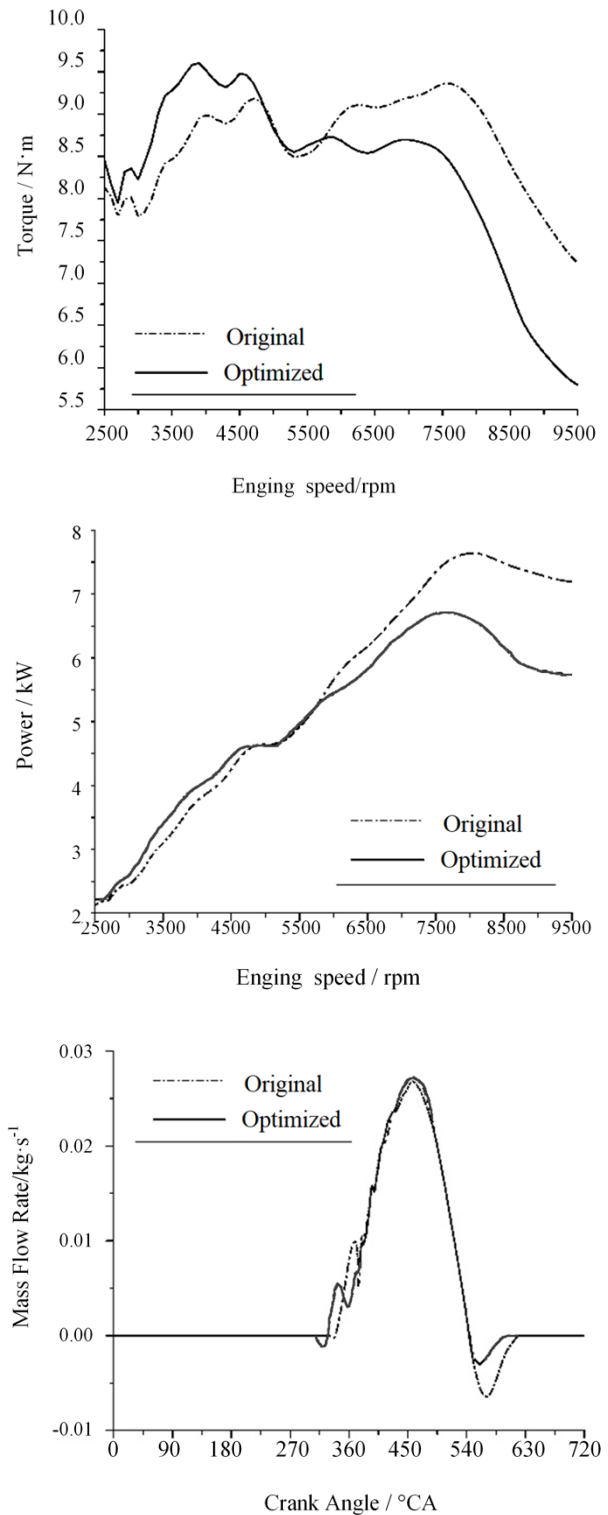


**Fig.11.** Comparison of torque, power, and intake mass flow rate after optimization at the engine speed of 4000 rpm

#### 4. Conclusions

The optimal results of the system with valve timing as independent variable and torque as output response are predicted based on experimental design and RSM. Before RSM optimization, PB experiment is used to distinguish the most basic variables, and a quadratic regression mathematical model is developed and verified to estimate the results of system optimization. The results show that the

method effectively predicts and improves the performance of fully variable valve train engine.

(1) The pressure wave and pulsating flow of intake and exhaust have nothing to do with valve timing. Therefore, the intake return flow is large due to this incongruity, and this condition negatively affects the performance of the engine.

(2) PB test shows that intake advance angle, intake duration angle, intake valve lift, and exhaust advance angle significantly affect the output response of braking torque, while variable timing and lift parameters insignificantly affect the BSFC of the engine at 4000 rpm.

(3) A quadratic regression model based on RSM is established with the four independent variables mentioned above. The interaction of these factors is analyzed from the contour and 3D maps of the RSM model, which indicates that the intake advance angle, intake duration angle, intake valve lift, and exhaust advance angle significantly affect the torque.

(4) The torque growth rate is 5.84%, while the BSFC remains nearly unchanged at 4000 rpm. The objective of

optimization is to conduct a certain engine speed. However, the optimization level of valve timing and valve lift is ideal compared with the original optimization level at 4800 rpm.

The engine valve parameters at constant speed are optimized in this study. This method can be further integrated to form a general model in the next step. It can be extended to the full speed situation, the variable behavior of valve parameters can be further guided, and the performance of the engine can be improved at different speeds and loads.

#### Acknowledgments

The authors would appreciate the support from National Natural Science Foundation of China (Grant No. 51405221)

This is an Open Access article distributed under the terms of the Creative Commons Attribution License.



#### References

- Pischinger, M., Salber, W., Der Staay, F.V., Baumgarten, H., Kemper, H. "Low fuel consumption and low emissions electromechanical valve train in vehicle operation". *International Journal of Automotive Technology*, 1(1), 2000, pp.17-25.
- Xu, J., Chang, S., Fan, X., Fan, A. "Effects of electromagnetic intake valve train on gasoline engine intake charging". *Applied Thermal Engineering*, 96, 2016, pp.708-715.
- Cleary, D., Silvas, G. "Unthrottled engine operation with variable intake valve lift, duration, and timing". *SAE Technical*, 2007-01-1282.
- Fan, X., Liu, L., Chang, S., Xu, J., Dai, J. "Electromagnetic valve train for gasoline engine exhaust system", *International Journal of Automotive Technology*, 17(3), 2016, pp.361-367.
- Sun, Z., Kuo, T.W. "Transient control of electro-hydraulic fully flexible engine valve actuation system". *IEEE Transactions on Control Systems Technology*, 18(3), 2010, pp.613-621.
- Liao, H., Roelle, M. J., Chen, J., Park, S., Gerdes, J.C. "Implementation and analysis of a repetitive controller for an electro-hydraulic engine valve system". *IEEE Transactions on Control Systems Technology*, 19(5), 2011, pp.1102-1113.
- Nam, K., Cho, K., Park, S., Choi, S.B. "Design and performance evaluation of an electro-hydraulic camless engine valve actuator for future vehicle applications", *Sensors (Basel)*, 17(12), 2017, pp.2940.
- Li, Q., Liu, J., Fu, J., Zhou, X., Liao, C. "Comparative study on the pumping losses between continuous variable valve lift (CVVL) engine and variable valve timing (VVT) engine", *Applied Thermal Engineering*, 137, 2018, pp.710-720.
- Sher, E., Bar-Kohany, T. "Optimization of variable valve-timing for maximizing performance of an unthrottled SI engine: a theoretical study". *Energy*, 27(8), 2002, pp.757-775.
- Yuan, Z., Fu, J., Liu, Q., Ma, Y., Zhan, Z. "Quantitative study on influence factors of power performance of variable valve timing (VVT) engines and correction of its governing equation". *Energy*, 157, 2018, pp. 314-326.
- Zhang, Y., Zhao, H. "Investigation of combustion, performance and emission characteristics of 2-stroke and 4-stroke spark ignition and CAI/HCCI operations in a DI gasoline". *Applied Energy*, 130(1), 2014, pp. 244-255.
- Peng, Z., Jia, M. "Full engine cycle cfd investigation of effects of variable intake valve closing on diesel pcci combustion and emissions". *Energy Fuels*, 23(12), 2009, pp. 5855-5864.
- Hong, H., Parvate-Patil, G.B., Gordon, B. "Review and analysis of variable valve timing strategies-eight ways to approach". *Proceedings of the Institution of Mechanical Engineers, Part D: Journal of Automobile Engineering*, 218(10), 2004, pp.1179-1200.
- Gölcü, M., Sekmen, Y., Erduranlı, P., Salman, S. "Artificial neural network based modelling of variable valve-timing in a spark-ignition engine". *Applied Energy*, 81, 2005, pp.187-197.
- Atashkari, K., Narimanzadeh, N., Gölcü, M., Khalkhali, A., Jamali, A. "Modelling and multi-objective optimization of a variable valve-timing spark-ignition engine using polynomial neural networks and evolutionary algorithms". *Energy Conversion and Management*, 48(3), 2007, pp.1029-1041.
- Zhao, J., Xu, M. "Fuel economy optimization of an Atkinson cycle engine using genetic algorithm". *Applied Energy*, 105, 2013, pp.335-348.
- Xin, Q. "Diesel engine system design". *Cambridge: Woodhead*, 2011.
- Kumar, A. N., Kishore, P. S., Raju, K. B., Ashok, B., Vignesh, R., Jeevanantham, A. K., Nanthagopal, K., & Tamilvanan, A. "Decanol proportional effect prediction model as additive in palm biodiesel using ANN and RSM technique for diesel engine". *Energy*, 213, 2020, pp. 119072.
- Uslu, S. "Optimization of diesel engine operating parameters fueled with palm oil-diesel blend: Comparative evaluation between response surface methodology (RSM) and artificial neural network (ANN)". *Fuel*, 276, 2020, pp.117990.
- Lopez, I., Pinzi, S., Leivacandia, D., Dorado, M.P. "Multiple response optimization to reduce exhaust emissions and fuel consumption of a diesel engine fueled with olive pomace oil methyl ester/diesel fuel blends". *Energy*, 117(2), 2016, pp.398-404.
- Hirkude, J., Padalkar, A.S. "Performance optimization of CI engine fuelled with waste fried oil methyl ester-diesel blend using response surface methodology". *Fuel*, 119, 2014, pp.266-273.
- Atmanli, A., Yuksel, B., Ileri, E., Karaoglan, A.D. "Response surface methodology based optimization of diesel-n-butanol-cotton oil ternary blend ratios to improve engine performance and exhaust emission characteristics". *Energy Conversion and Management*, 90, 2015, pp.383-394.
- Awad, O.I., Mamat, R., Ali, O.M., Azmi, W.H., Kadrigama, K., Yusri, I.M., Leman, A.M., Yusaf, T. "Response surface methodology (RSM) based multi-objective optimization of fusel oil-gasoline blends at different water content in SI engine". *Energy Conversion and Management*, 150, 2017, pp. 222-241.
- Alimohammadi, H. R., H. Naseh, and F. Omimi. "A novel framework for liquid propellant engine's cooling system design by sensitivity analysis based on RSM and multi-objective optimization using PSO". *Advances in Space Research*, 67(5), 2020, pp. 1682-1700.